Proceedings of the Institute of Acoustics

MODELS FOR SCATTERING FROM THE SEA BED

D R Jackson

Applied Physics Laboratory, University of Washington, Seattle, Washington, USA

1. INTRODUCTION

The models for scattering from the sea bed to be discussed in this paper are extensions of a model for high-frequency backscatter strength presented by Jackson et al. in 1986 [1]. The models to be treated are intended for use at high frequencies (10–100 kHz). First, an improved backscatter model will be outlined in the form presented by Mourad and Jackson [2] and employed by Jackson and Briggs [3]. Second, a bistatic generalization of this model will be presented in some detail. References to prior work by other investigators can be found in the papers cited above.

2. OUTLINE OF BACKSCATTER MODEL

The backscatter model treats scattering due to both roughness of the sea bed and volume inhomogeneities of the sediment [4]. Accordingly, the backscattered intensity is assumed to be a sum of two terms, one proportional to the roughness scattering cross section and the other proportional to the volume scattering cross section. It is assumed that the acoustic penetration of the sea bed is slight, so that sediment volume scattering can be described as a surface process and quantified by an effective interface scattering cross section.

A major assumption in this model is that the sediment can be treated as a lossy fluid; any effects due to elasticity or porosity are neglected. It is further assumed that there are no gradients in sediment properties, apart from the random fluctuations responsible for volume scattering. Thus, the sediment can be characterized by three parameters: mass density, sound speed, and acoustic absorption coefficient. The sea bed relief is assumed to be an isotropic, two-dimensional Gaussian random process completely determined by a spectral density that follows a simple power law in wavenumber. This adds two more parameters to the model: the exponent of the power law and a parameter that sets the overall spectral level. Scattering from interface roughness is computed by a combination of the composite roughness [5] and Kirchhoff approximations. This requires that the interface not be too rough, although the precise constraints on allowable roughness are not well understood. Finally, sediment volume scattering is characterized by a strength parameter. The volume scattering strength is assumed to be omnidirectional and depth independent. Volume scattering is assumed to be weak in the sense that the scattered field is much smaller in magnitude than the incident field (defined as the field that would exist in the sediment in the absence of volume scattering).

Figure 1 shows a typical result for sea bed backscattering strength (defined as in Urick [6]) obtained using this model. This computation employed model parameters appropriate to a medium sand sediment. The definition of the parameters listed in the figure caption will be given later. In this example, scattering due to interface roughness dominates sediment volume scattering for small and large grazing angles. There is a peak in the roughness scattering component near the critical angle (32° in this example). This peak is a typical feature of the small-roughness perturbation approximation when applied to the rough fluid-fluid boundary. The composite roughness approximation averages the perturbation result with respect to

random sea bed slope and also introduces a shadowing factor. Figure 2 shows that these are small corrections to the perturbation result, except at very small grazing angles. For angles greater than the critical angle, acoustic energy is able to penetrate the sediment, and sediment volume scattering becomes important (Fig 1.). As the grazing angle approaches 90° (vertical incidence), roughness scattering again dominates. This is essentially reflection of vertically directed energy, with some angular spreading due to interface roughness. This portion of the scattering strength curve is computed using the Kirchhoff approximation. Use of the high-frequency limit of the Kirchhoff approximation (variously referred to as the 'geometric optics', 'facet', or 'broken mirror' model) is avoided, as the high-frequency limit neglects diffractive effects which strongly affect the shape and frequency dependence of the near-vertical scattering strength curve [7].

References [1]–[3] compare the backscatter model with data from seven well-characterized sites. At these sites, measurements were available for sediment mass density, sound speed, sound absorption coefficient, and roughness spectrum. The only model parameter not measured was the sediment volume scattering strength, which was treated as a free parameter in comparisons of the model and data. The data set included sediments ranging from medium sand to finer grained sands, silts and clays. The sandy sea beds could be described as acoustically 'hard', with substantial contrast in density and sound speed relative to the sea water. In these cases, the measured roughness alone accounted for the observed scattering strengths, with typical differences of 3 dB between model and data and occasional differences of about 6 dB. For the 'softer' silt and clay sea beds, the roughness scattering component of the model typically fell 15 dB or more below the data. In these cases, the volume scattering strength of the sediment was adjusted to fit the data. The resulting model curves provided a good one-parameter fit to the data, indicating that sediment volume scattering was dominant at these sites.

It is well known that Lambert's 'law' (in which backscattering strength is equal to the squared sine of the grazing angle expressed in decibels plus an arbitrary constant) often provides a good fit to sea bed backscattering data at small grazing angles [8],[9]. Our modeling work suggests that this is fortuitous in that roughness and volume scattering mechanisms working together tend to mimic Lambert's law. This point is illustrated by Fig. 1 in which Lambert's law is compared with the model results. Lambert's law must obviously fail as the grazing angle approaches 90°, where the scattering strength curve has a sharp peak. Even so, Lambert's law is an approximate experimental fact at small angles; consequently, it is interesting to compare Lambert's law with the backscatter model for a wide class of sea bed types. This is done in Fig. 3, which gives the minimum rms difference between Lambert's law and the model for a fit over the angular range 3–20°. The horizontal axis of the figure is mean grain size expressed in commonly used base-2 logarithmic units. In these units, a mean sediment grain diameter of 1 mm corresponds to a logarithmic value of 0 ϕ and is the size boundary between very coarse sand and coarse sand. A diameter of 2 mm (the size boundary between gravel and sand) corresponds to a logarithmic value of -1 ϕ, and a diameter of 1/16 mm (the size boundary between sand and silt) corresponds to a logarithmic value of 4 ϕ. Mourad and Jackson [2] provide relationships between mean grain diameter and model input parameters. These relationships should be viewed as defaults to be used in the absence of measured sediment physical properties. In the present case, these relationships provide a convenient means of spanning a wide range of parameter space while remaining within physically reasonable bounds. In the fitting process, a model curve was computed for a given grain size, a minimum mean-square error fit of Lambert's law over the angular range 3–20° was then carried out, the rms difference was computed, grain diameter was incremented, etc. As Fig. 3 shows, the fit provided by Lambert's law is quite good, with an rms difference less than 1 dB except in the interval 2–4 ϕ (fine to very fine sand), where the difference rises to values between 1.5 and 2.5 dB. This increased difference is due to the critical angle effects discussed earlier, which cause the model curve to depart from a Lambert shape.

Comparisons between the backscatter model and data encourage further development of this approach. The bistatic generalization to be described next employs the same basic assumptions regarding interface roughness and the treatment of sediments as lossy fluids.

3. BISTATIC MODEL DEFINITIONS

The backscatter model just outlined has been generalized to cover bistatic scattering in all directions. This generalization adheres to the previously given assumptions with a few exceptions noted below.

The bistatic scattering strength will be written in the form

$$S_b (\theta_s, \phi_s, \theta_i) = 10 \log_{10} [\sigma_{br} (\theta_s, \phi_s, \theta_i) + \sigma_{bv} (\theta_s, \phi_s, \theta_i)] \ , \qquad (1)$$

where $\sigma_{br} (\theta_s, \phi_s, \theta_i)$ and $\sigma_{bv} (\theta_s, \phi_s, \theta_i)$ are the roughness and volume contributions to the scattering cross section per unit area. The angles θ_s, ϕ_s, and θ_i are defined in Fig. 4. The 'incident grazing angle' is denoted θ_i, the 'scattered grazing angle' is θ_s, and ϕ_s is the 'bistatic angle', defined as the the difference in azimuth between the incident and scattered directions. In general, one needs *four* angles, two grazing angles and two azimuths, but only the azimuthal difference is needed here, because bottom statistics are assumed to be transversely isotropic. Later expressions for the scattering cross section will employ the following geometric parameters:

$$\Delta_t = \frac{1}{2} (\cos^2\theta_i - 2 \cos\theta_i \cos\theta_s \cos\phi_s + \cos^2\theta_s)^{1/2} \ , \qquad (2)$$

and

$$\Delta_z = \frac{1}{2} (\sin\theta_i + \sin\theta_s) \ . \qquad (3)$$

These dimensionless parameters are proportional, respectively, to the transverse and vertical components of the change in acoustic wave vector upon scattering. A parameter proportional to the magnitude of the change is also used.

$$\Delta = \sqrt{\Delta_t^2 + \Delta_z^2} \ . \qquad (4)$$

Like the backscatter model, the bistatic model treats the sediment as a fluid, homogeneous except for fluctuations responsible for volume scattering. The fluid properties are defined by three dimensionless mean ratios, ρ, v, and δ. These are, respectively, the sediment/water density ratio, the sediment/water sound speed ratio, and the ratio of imaginary to real wavenumber in the sediment.

The backscatter model uses the Kirchhoff approximation near vertical incidence, and the bistatic model analogously uses this approximation near the specular direction. In other directions, the bistatic model employs the small-roughness perturbation approximation. Unlike the backscatter model, the composite-roughness approach is not used to improve the perturbation result. This is primarily for reasons of simplicity, but also because the composite-roughness corrections are usually small (Fig. 2) and of uncertain accuracy. The input parameters describing bottom roughness are identical to those for the backscatter model, which uses a two-parameter, isotropic two-dimensional roughness spectral density:

$$W(K) = \frac{w_2}{(h_0 K)^{\gamma_2}} , \tag{5}$$

where K is the magnitude of the two-dimensional wave vector and the spectrum is normalized so that the integral over a finite region in K–space gives the mean-square vertical deviation of the sea bed from the mean plane due to those Fourier components included in the integration. The exponent is restricted to the range

$$2 < \gamma_2 < 4 . \tag{6}$$

The parameter w_2 gives the strength of the spectrum and has dimensions (length)^4. The parameter h_0 is simply a reference length needed to balance dimensions in Eq. 5. It is assigned the numerical value 1, and hence does not appear in calculations.

The volume scattering portion of the older backscatter model is phenomenological in that it employs an empirical volume scattering strength as an input. This approach could be generalized to the bistatic case by assigning the volume scattering strength an arbitrary angular dependence, but such a model would have little predictive capability. For the bistatic model, a more physical approach is adopted, using perturbation theory for volume scattering along the lines developed by Ivakin and Lysanov [10], Hines [11], Tang [12], and Lyons and Anderson [13]. Where the older backscatter model employed a single parameter to quantify sediment volume scattering strength, the bistatic model requires three parameters to characterize spectra for inhomogeneities in density and compressibility. The spectrum for density fluctuations is taken to be of the same power-law form as the roughness spectrum:

$$W_{\rho\rho}(k) = \frac{w_3}{(k h_0)^{\gamma_3}} . \tag{7}$$

This spectrum is isotropic and normalized such that an integral over a finite volume of k-space yields the mean-square density fluctuation divided by the square of the mean density. Compressibility fluctuations are treated analogously and are assumed to be proportional to the density fluctuations. Thus, the spectrum of compressibility fluctuations is

$$W_{KK} = \mu^2 W_{\rho\rho} , \tag{8}$$

and the cross spectrum is

$$W_{\rho K} = \mu W_{\rho\rho} , \tag{9}$$

where μ is a dimensionless parameter, to be discussed later.

4. BISTATIC ROUGHNESS SCATTERING

In this section, expressions will be presented for the bistatic cross sections in the Kirchhoff and perturbation approximations. The net cross section, $\sigma_{br}(\theta_s, \phi_s, \theta_i)$, appearing in Eq. 1 is formed by smooth interpolation between the Kirchhoff cross section near the specular direction and the perturbation theory cross section elsewhere. The following cross section expressions are standard results, expressed here in notation convenient to the bistatic application.

4.1 Kirchhoff Approximation

Analogous to the monostatic expression used by Jackson et al. [1], the bistatic Kirchhoff cross section [14],[15] can be expressed in the following form:

$$\sigma_{kr}(\theta_i, \phi_s, \theta_i) = \frac{|R(\theta_{is})|^2}{8\pi}\left[\frac{\Delta^2}{\Delta_z \Delta_t}\right]^2 \int_0^\infty e^{-q u^{2\alpha}} J_0(u)\, u\, du \ , \tag{10}$$

where

$$q = 2 k^2 \Delta_z^2 C_h^2 (2 k \Delta_t)^{-2\alpha} \ . \tag{11}$$

In Eqs. 10 and 11, $J_0(u)$ is the zeroth-order Bessel function of the first kind and k is the acoustic wavenumber in water. The parameters α and C_h are roughness structure function parameters related to γ_2 and w_2 as follows:

$$\alpha = \frac{\gamma_2}{2} - 1 \ , \tag{12}$$

and

$$C_h^2 = \frac{2\pi w_2 \Gamma(2-\alpha) 2^{-2\alpha}}{h_0^{\gamma_2}\, \alpha(1-\alpha)\Gamma(1+\alpha)} \ . \tag{13}$$

The function $R(\theta_{is})$ is the complex plane-wave reflection coefficient (the so-called Rayleigh or Fresnel reflection coefficient) for a flat interface separating water and sediment. It can be expressed in terms of the parameters ρ, v, and δ [2] and is evaluated at the grazing angle

$$\theta_{is} = \sin^{-1}\Delta \ . \tag{14}$$

This angle is not the actual incident or scattered grazing angle relative to the horizontal; rather, it is the grazing angle that would result if the bottom were tipped in such a way as to provide specular reflection between the transmitter and receiver. Thorsos (private communication) finds that this value gives improved accuracy compared to other choices, as reflection from suitably oriented facets tends to dominate the scattering process near the specular direction.

4.2 Perturbation Approximation

The bistatic backscattering cross section computed in the perturbation approximation [1]–[3],[16] can be put in the following form:

$$\sigma_{pr}(\theta_i, \phi_s, \theta_i) = \frac{1}{4} k^4 \mid 1 + R(\theta_i) \mid^2 \mid 1 + R(\theta_s) \mid^2 \mid G \mid^2 W(2k\Delta_t) \ , \tag{15}$$

Equation 15 involves the reflection coefficient and roughness spectral density discussed earlier. The argument of the roughness spectral density is the 'Bragg wavenumber'. The complex function G is

$$G = (1/\rho - 1)[\cos\theta_i \cos\theta_s \cos\phi_s - P(\theta_i) P(\theta_s)/\rho] + 1 - \kappa^2/\rho \ . \tag{16}$$

In Eq. 16,

$$\kappa = \frac{1 + i\delta}{v} \tag{17}$$

is the complex wavenumber in the sediment divided by the real wavenumber in water and

$$P(\theta) = \sqrt{\kappa^2 - \cos^2\theta} \ . \tag{18}$$

5. SEDIMENT BISTATIC VOLUME SCATTERING

Mourad and Jackson [2] used a volume scattering expression similar to that of Stockhausen [17] in their backscatter model. The bistatic equivalent is readily obtained. It relates the sediment volume scattering cross section σ_v to the effective interface bistatic scattering cross section, $\sigma_{bv}(\theta_s, \phi_s, \theta_i)$, appearing in Eq. 1.

$$\sigma_{bv}(\theta_s, \phi_s, \theta_i) = \frac{\sigma_v \mid 1 + R(\theta_i) \mid^2 \mid 1 + R(\theta_s) \mid^2}{2k\rho^2 \ \mathrm{Im}\left\{ P(\theta_i) + P(\theta_s) \right\}} \ . \tag{19}$$

Perturbation theory is used to obtain the volume scattering cross section, σ_v. Adapting a result given by Ishimaru [18] to the present situation, and using Eqs. 7–9, yields

$$\sigma_v = \frac{\pi}{2} k^4 \mid \mu\kappa^2 + \cos\theta_i \cos\theta_s \cos\phi_s - P(\theta_i) P(\theta_s) \mid^2 W_{pp}(\Delta k) \ . \tag{20}$$

Sediment acoustic loss has been included by allowing the wavenumber in the bottom to be complex. The spectrum W_{pp} is evaluated at the Bragg wavenumber for volume scattering, which is the magnitude of the difference between the real parts of the incident and scattered three-dimensional wavevectors (defined in the sediment).

$$\Delta k = k \left[4 \Delta_i^2 + \left(\mathrm{Re} \; P(\theta_i) + P(\theta_s) \right)^2 \right]^{1/2} . \tag{21}$$

The dimensionless volume scattering parameter used in the backscatter model [2] and appearing in the caption of Fig. 1 can be expressed in terms of the bistatic model parameters as follows:

$$\sigma_2 = \frac{\pi \ln 10}{40 \delta} (2 h_0)^{-\gamma_3} w_3 (k/\nu)^{3-\gamma_3} (1 + \delta^2)^2 (\mu - 1)^2 \tag{22}$$

6. COMPARISONS WITH PUBLISHED DATA

Williams and Jackson [19] have reported preliminary comparisons of the present bistatic model with their experimental data, with promising results. The experimental literature on bistatic scattering by the sea bed is sparse and not generally in a form useful for rigorous tests of models, but the data of Hurdle et al. [20], Urick [21], and Stanic et al. [22] are useful in this regard.

The bistatic model is compared with some of the data of Hurdle et al. [20] in Fig. 5. Their measurements were made at a frequency of 19.5-kHz on the East Bermuda rise. Site 1 had a 'mud-coral' bottom and a depth of 750 fathoms, and Site 2 had an 'ooze' bottom and a depth of 1250 fathoms. No physical data on bottom properties are available for these sites, so default parameters appropriate to a silt bottom were used. These are $\rho = 1.15$, $\nu = 0.987$, $\delta = 0.00386$, $\gamma_2 = 3.25$, $w_2 = 0.000518$ cm^4, $\gamma_3 = 3.0$, $w_3 = 0.000306$ cm^3, and $\mu = -1.0$. This choice for μ amounts to the assumption that the fractional fluctuations in density and compressibility are equal and opposite. This is a plausible assumption, as it results in negligible sound speed fluctuations. While observation indicates that sound speed fluctuations are nonzero, they tend to be much smaller than density fluctuations on a fractional basis. The choice $\gamma_3 = 3.0$ removes all frequency dependence for sediment volume scattering, as suggested by backscatter data for soft sediments [3], [23], [24]. The inhomogeneity strength parameter, w_3, has been assigned a value consistent with the measured scattering strengths of Hurdle et al.

In the model/data comparison of Fig. 5, the bistatic angle is fixed at 180°, and the scattered grazing angle is the independent variable. In this example, the model scattering strength is due to sediment volume scattering, except for the near-specular peak, which results from interface scattering. The model and data agree reasonably well in directions away from specular, but the data do not exhibit the sharp specular peak predicted by the model. This may be due to the smearing effect of the 8° beamwidth of the source or it may indicate that the sea bed had a smaller reflection coefficient than implied by the assumed parameters.

Urick [21] measured bistatic scattering at 22 kHz at a shallow (10–20 m) site near Panama City, Florida. The transmitter and receiver were near the bottom and separated by about 3 km. Both transmitter and receiver were directional and were pointed in various directions to provide scattering strength measurements over a range of bistatic angles (ϕ_s in the present notation). Because the transmitter/receiver separation was much greater than the water depth, multipathing must have been very complicated, with the result that both incident and scattered grazing angles are ill defined. In order to compare Urick's data with the present model, it will be assumed that the incident and scattered grazing angles were small, and a value of 10° will be used, somewhat arbitrarily. Since the site was not characterized, parameters appropriate to a sandy sea bed will be employed: $\rho = 1.94$, $\nu = 1.113$, $\delta = 0.0115$, $\gamma_2 = 3.67$, $w_2 = 0.00422$ cm^4, $\gamma_3 = 3.0$, $w_3 = 0.000127$ cm^3, and $\mu = -1.0$. Figure 6 shows

that the model and data are in qualitative agreement in exhibiting no strong dependence on bistatic angle over the range of interest, which does not include angles near the specular direction. The approximate agreement in *level* of scattering strength must be considered fortuitous, given the uncertainties in grazing angle and model input parameters. Nevertheless, this appears to be a useful comparison as regards the lack of dependence on the bistatic angle for angles ranging from the backscatter direction to within 30° of specular.

Further qualitative confirmation of the model near the backscatter direction is provided by the data of Stanic et al. [22] from a sandy site near Jacksonville, Florida. Their data cover a wide frequency range (20–180 kHz) and incident grazing angles from 8.8° to 28°. The focus of their work was the statistical fluctuation of the scattered energy; they do not give absolute scattering strength values. One can infer angular dependence (or lack of it) from their data, however. The bistatic angles covered a range within 9° of the backward direction at the largest incident grazing angles and about half that range at the smallest. The scattered grazing angles covered a range within 2° or less of the backward direction. The data show no clear trend with either angle, from which it is inferred that the bistatic scattering strength was essentially constant over the angular range cited above. This agrees with the general behavior of the model near the backscatter direction (Fig. 6).

Acknowledgments. This work was supported by the Office of Naval Research.

7. REFERENCES

[1] D R Jackson, D P Winebrenner & A Ishimaru, 'Application of the Composite Roughness Model to High-Frequency Bottom Backscattering', J Acoust Soc Am, 79, p1410, 1986.
[2] P D Mourad & D R Jackson, 'High Frequency Sonar Equation Models for Bottom Backscatter and Forward Loss', Proc. OCEANS '89, p1168, 1989.
[3] D R Jackson & K B Briggs, 'High-Frequency Bottom Backscattering: Roughness Versus Sediment Volume Scattering', J Acoust Soc Am, 92, p962, 1992.
[4] P A Crowther, 'Some Statistics of the Sea-bed and Scattering Therefrom', in Acoustics and the Sea Bed, edited by N G Pace (Bath University, Bath, 1983), p147.
[5] S T McDaniel & A D Gorman, 'Acoustic and Radar Sea Surface Backscatter', J Geophys Res, 87, p4127, 1982.
[6] R J Urick, Principles of Underwater Sound (McGraw-Hill, New York, 1983).
[7] S T McDaniel, 'Diffractive Corrections to the High-Frequency Kirchhoff Approximation', J Acoust Soc Am, 79, p952, 1986.
[8] S Stanic, K B Briggs, P Fleischer, R I Ray, & W B Sawyer, 'Shallow-Water High-Frequency Bottom Scattering Off Panama City, Florida', J Acoust Soc Am, 83, p2134, 1988.
[9] H Boehme & N P Chotiros, 'Acoustic Backscattering At Low Grazing Angles From the Ocean Bottom', J Acoust Soc Am, 84, p1018, 1988.
[10] A N Ivakin & Yu P Lysanov, 'Underwater Sound Scattering by Volume Inhomogeneities of a Bottom Medium Bounded by a Rough Surface', Sov Phys Acoust, 27, p212, 1981.
[11] P C Hines, 'Theoretical Model of Acoustic Backscatter From a Smooth Seabed', J Acoust Soc Am, 88, p324, 1990.
[12] D Tang, 'Acoustic Wave Scattering From a Random Ocean Bottom', PhD thesis, Massachusetts Institute of Technology and Woods Hole Oceanographic Institution, June 1991.
[13] A P Lyons & A L Anderson, 'Acoustic Scattering From the Seafloor: Modeling and Data Comparison', J Acoust Soc Am, 95, p2441, 1994.

[14] A Ishimaru, Wave Propagation and Scattering in Random Media, Volume 2 (Academic Press, New York, 1978).
[15] E I Thorsos, 'The Validity of the Kirchhoff Approximation for Rough Surface Scattering Using a Gaussian Roughness Spectrum', J Acoust Soc Am, 83, p78, 1988.
[16] E Y Kuo, 'Wave Scattering and Transmission at Irregular Surfaces', J Acoust Soc Am, 36, p2135, 1964.
[17] J H Stockhausen, 'Scattering From the Volume of an Inhomogeneous Half-Space', Report No. 63/9, Naval Research Establishment, Canada, 1963.
[18] A Ishimaru, Wave Propagation and Scattering in Random Media, Volume 1 (Academic Press, New York, 1978).
[19] K Williams & D Jackson, 'Monostatic and Bistatic Bottom Scattering: Recent Experiments and Modeling', to appear in Proceedings OCEANS '94, 1994.
[20] B G Hurdle, K D Flowers & K P Thompson, 'Bistatic Acoustic Scattering From the Ocean Bottom', NRL Report 7285, 1971.
[21] R J Urick, 'Side Scattering of Sound in Shallow Water', J Acoust Soc Am, 32, p351, 1960.
[22] S Stanic, E Kennedy & R I Ray, 'Variability of Shallow-Water Bistatic Bottom Backscattering', J Acoust Soc Am, 90, p547, 1989.
[23] D R Jackson, A M Baird, J J Crisp & P A G Thomsom, 'High-Frequency Bottom Backscattering Measurements in Shallow Water', J Acoust Soc Am, 80, p1188 1986.
[24] M Gensane, 'A Statistical Study of Acoustic Signals Backscattered From the Sea Bottom', IEEE J Oceanic Eng, 14, p84, 1989.

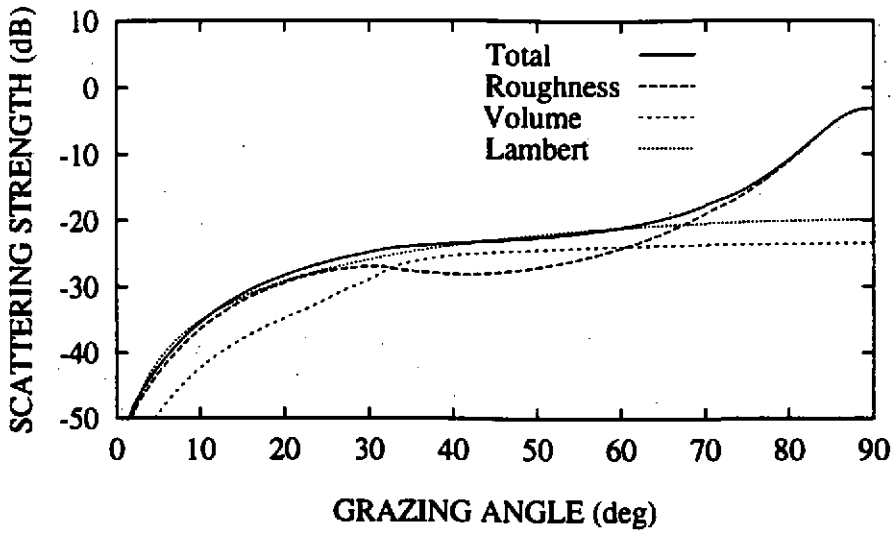

Fig. 1. Model curves at 30 kHz for sea bed backscattering strength vs grazing angle. The solid curve is the model result using input parameters appropriate to a medium sand sea bed ($\rho = 1.845$, $v = 1.1782$, $\delta = 0.01624$, $\sigma_2 = 0.002$, $\gamma_2 = 3.25$, $w_2 = 0.004446$). The two dashed curves show the contributions of the roughness and volume scattering components of the model. The dotted curve is Lambert's law fitted over the angular range 3°–20°.

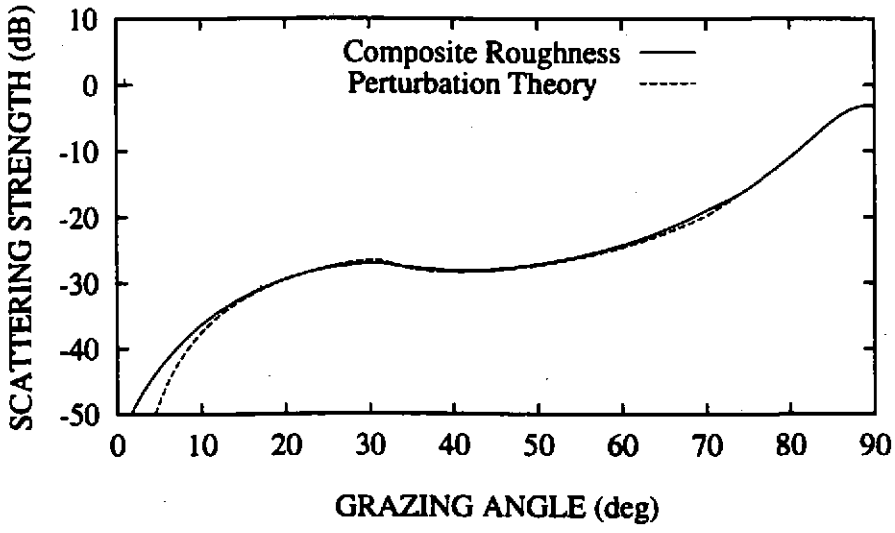

Fig. 2. Comparison of perturbation and composite-roughness calculations for roughness scattering using the same parameters as for Fig. 1.

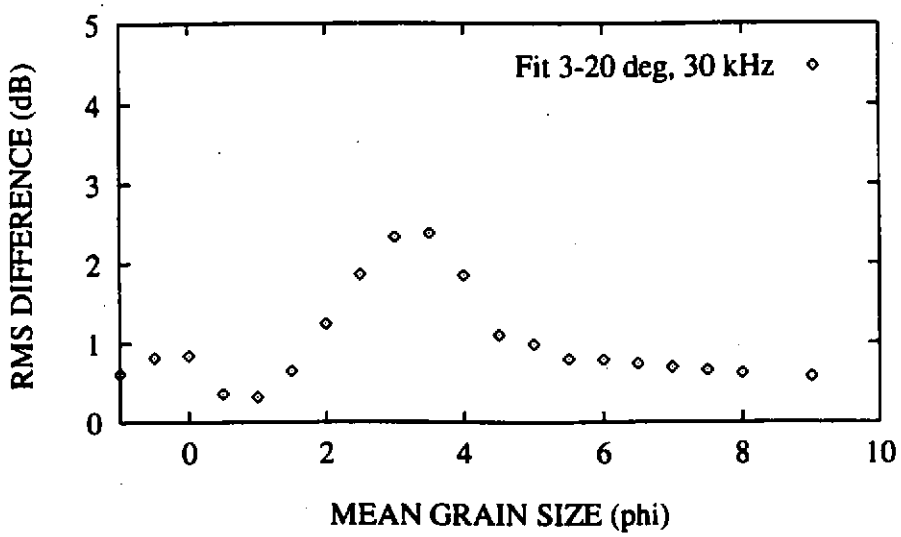

Fig. 3. Minimum rms difference between Lambert's law and the backscatter model for various sea bed types.

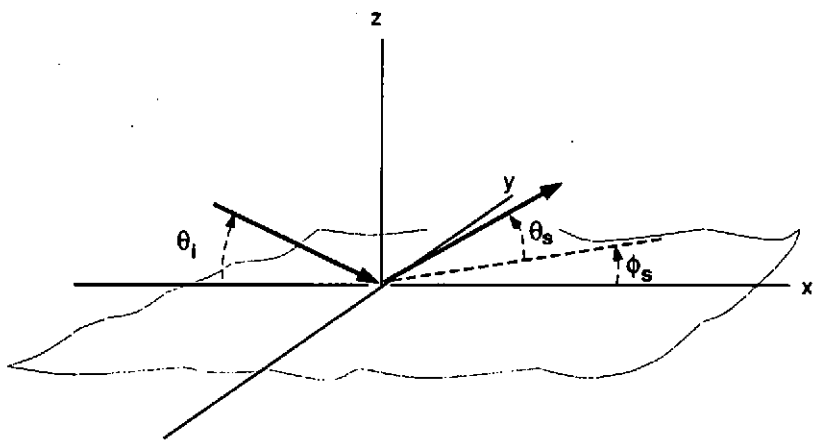

Fig. 4. Bistatic scattering geometry. The incident and scattered directions are denoted by arrows. The angle θ_i is the incident grazing angle, θ_s is the scattered grazing angle, and ϕ_s is the bistatic angle.

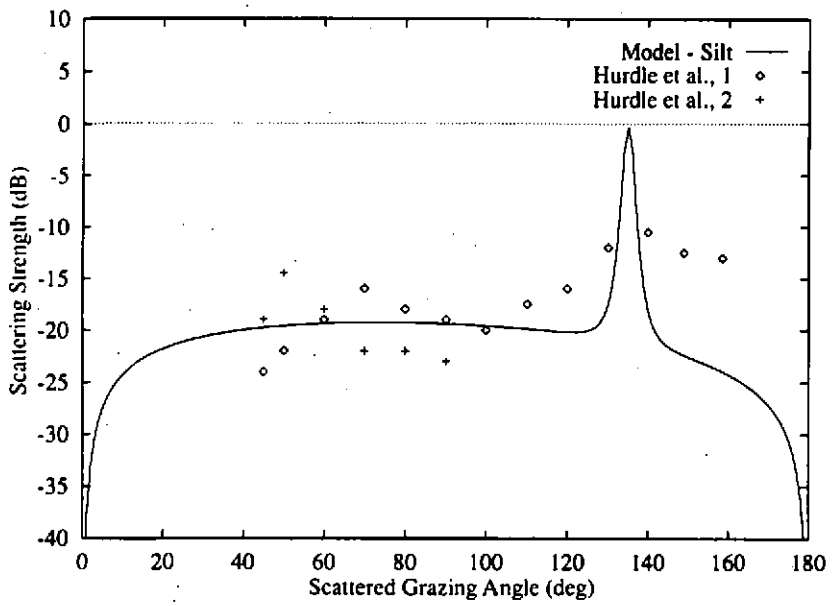

Fig. 5. Comparison of bistatic model with 19.5-kHz data from stations 1 and 2 of Hurdle et al. [20]. The bistatic angle is fixed at 180°, and the incident grazing angle is 45°. The x-axis is scattered grazing angle, ranging from 0° (horizontal scattering) through 90° (vertical scattering) to 180° (horizontal scattering).

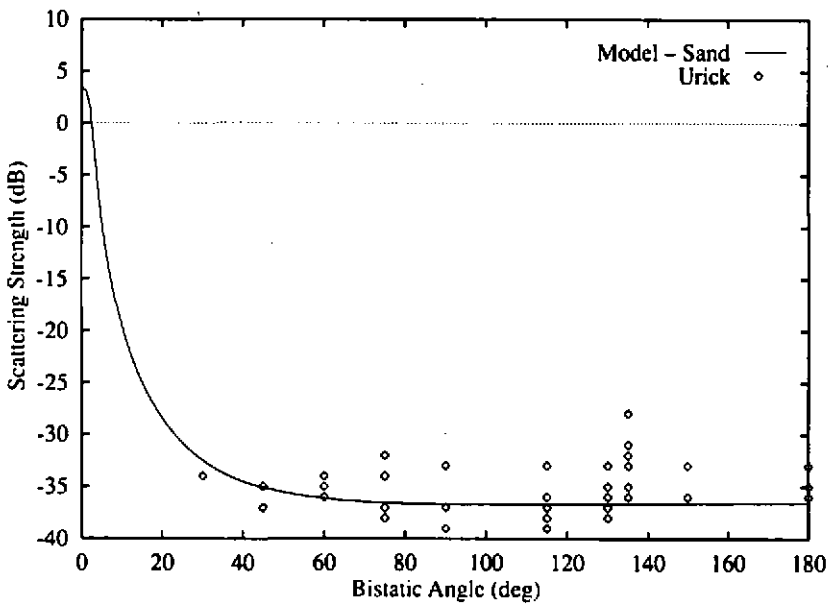

Fig. 6. Comparison of bistatic model with 22-kHz data of Urick [21]. The incident and scattered grazing angles are fixed at 10°, and the x-axis is bistatic angle, ranging from 0° (specular direction) to 180° (backscattering).